Available online at www.sciencedirect.com
ScienceDirect
Journal of Non-Crystalline Solids 353 (2007) 2459–2468
JOURNAL OF NON-CRYSTALLINE SOLIDS
www.elsevier.com/locate/jnoncrysol

Continuous compositional changes of crystal and liquid during crystallization of a sodium calcium silicate glass

V.M. Fokin [a,*], E.D. Zanotto [b]

[a] S.I. Vavilov's State Optical Institute, ul. Babushkina 36/1, St. Petersburg 192131, Russia
[b] Vitreous Materials Laboratory, Federal University of São Carlos, 13565-905 São Carlos, SP, Brazil

Received 17 September 2006; received in revised form 20 December 2006

Abstract

This paper deals with a systematic study of crystal nucleation and growth kinetics in a $14.6Na_2O$–$34.0CaO$–$51.4SiO_2$ mol% glass, which is close to the $CaO \cdot SiO_2$–$Na_2O \cdot SiO_2$ pseudo-binary section, just left of the stoichiometric $Na_2O \cdot 2CaO \cdot 3SiO_2$ ($N_1C_2S_3$) compound. We show that crystallization begins with nucleation of a $Na_{4+2x}Ca_{4-x}[Si_6O_{18}]$ ($0 < x < 1$) solid solution that is enriched in sodium as compared with both parent glass and the $N_1C_2S_3$ compound; while a fully crystallized sample is composed only by a solid solution that is stable at very high temperatures, but is metastable in the temperatures under investigation. We thus confirm a continuous compositional change of the *crystals* during the course of crystallization.

PACS: 64.70.Kb; 64.60.Qb

Keywords: Crystallization; Crystal growth; Glass ceramics; Nucleation

1. Introduction

The thermodynamic barrier for nucleation or the work for critical nucleus formation, W_*, to a great extent determines the nucleation rate in supercooled liquids. For this reason, to use any nucleation theory one must first define the composition, structure and thermodynamic properties of the critical nucleus to evaluate W_*. This task, and especially its experimental solution, is not trivial due to the extremely small critical nucleus sizes (only a few nanometers) at the deep undercoolings needed to attain detectable homogeneous nucleation in typical glass forming liquids. This is one of the reasons why the newly evolving macrophase (predicted by the respective equilibrium phase diagram) is commonly used as a reference to describe the properties of the critical nucleus. This approach is consistent with assumptions of the classical nucleation theory (CNT) employing Gibbs' description of heterogeneous systems. However, a maximum thermodynamic driving force, i.e. that of the stable phase, is not a necessary condition to attain the minimum value of the thermodynamic barrier and maximum nucleation rate, because W_* is a combination of the thermodynamic driving force, ΔG_V, for crystallization and the specific surface energy, $\sigma_{c/l}$, of the nucleus/liquid interface:

$$W_* \sim \frac{\sigma_{c/l}^3}{\Delta G_V^2}. \quad (1)$$

Particularly, preferred nucleation of the phase having the lowest thermodynamic barrier rather than other thermodynamically possible phases is the basis of the kinetic argumentation of *Ostwald's rule of stages*, according to which any system prefers to reach intermediate stages having the closest free energy difference to the initial state [1]. Thus, some serious problems that often arise during quantitative analyses of nucleation data in the framework of CNT (e.g. see [2]) could be caused, at least in part, by the

* Corresponding author. Tel.: +7 812 355 30 38.
E-mail address: vfokin@pisem.net (V.M. Fokin).
URL: www.lamav.ufscar.br (E.D. Zanotto).

0022-3093/$ - see front matter © 2007 Elsevier B.V. All rights reserved.
doi:10.1016/j.jnoncrysol.2007.04.014

erroneous employment of ΔG_V for crystallization of the stable macro-phase for the critical nuclei using the specific surface energy as a fitting parameter. Indeed, in the last decade, indirect and direct experimental evidences appeared pointing out to the difference between the critical (and near critical) nuclei, and the corresponding stable macro-phase. Some of these evidences are listed below:

(a) A strong discrepancy between the time-lags for nucleation estimated from crystal nucleation and growth kinetics [3,4] in lithium silicate glasses with compositions between di- and metasilicate.
(b) Discrepancy between the $\sigma_{c/l}$ estimated from the nucleation rate, and from the effect of dissolution of sub-critical nuclei as the temperature increases [5]. This problem could be avoided by assuming that the thermodynamic driving force is smaller than that for macro-phase crystallization.
(c) Crystallization of sodium–calcium silicate glasses (in particular of the stoichiometric composition $Na_2O \cdot 2CaO \cdot 3SiO_2$) by nucleation of solid solutions whose composition continuously varies during the phase transformation [6,7] approaching the composition of the stable phase only in the end.
(d) A remarkable size-dependence of the cluster composition has also been observed during primary crystallization of NiP particles in a hypoeutectic Ni–P amorphous alloy [8]. In this case, the compositional evolution was completed when the clusters attained about 10 nm.
(e) Variation of (micron size) crystal compositions with the degree of undercooling was found recently in $CaO–Al_2O_3–SiO_2$ glasses [9] where it was demonstrated, that equilibrium crystals form near the *liquidus*, while disordered and non-stoichiometric phases precipitate near the glass transition temperature. This finding corroborates the statement that 'metastable crystalline phases commonly precipitate in the initial stage of low-temperature crystallization of multicomponent glasses' made in Ref. [10].
(f) A size-dependence of the crystal composition has also been detected for crystals formed on the surface of a cordierite glass [11].

The above mentioned results are still not numerous. This situation is due to the fact that most authors do not pay attention to the exact *composition* of the crystalline phases that precipitate in undercooled liquids, especially in the initial stages of phase transformation. However, one can expect that the compositional and structural evolution of the crystalline phase during phase transformation is a general feature. Therefore, the search and study of such phenomenon are of great interest from both theoretical and practical points of view since they may help one to find out a realistic approach for the nucleation process in glasses. In particular, from these evidences it became clear that the choice of stoichiometric glass compositions as model systems does not guarantee that the crystal nuclei will have the same composition as the parent glass, i.e. the condition needed to treat the studied system as 'one-component' (or stoichiometric) is not necessarily fulfilled in this way.

This paper presents additional experimental evidence for a continuous evolution of the *crystal* composition during nucleation and growth in a sodium–calcium silicate glass, extending the composition interval studied earlier and described in Refs. [12,13]. In addition, existing crystal nucleation rates are analyzed and compared with our own as a function of glass composition and reduced glass transition temperature.

2. Materials and methods

We employed sodium and calcium carbonates, and amorphous silicon dioxide of analytical grade for the glass synthesis. The melt was cast on a massive steel plate after about 2 h at 1450 °C in a platinum crucible. The glass composition by analysis ($14.6Na_2O–34.0CaO–51.4SiO_2$ mol%) is close to the pseudo-binary meta silicate section $CaO \cdot SiO_2–Na_2O \cdot SiO_2$ and lies just left of the stoichiometric compound $Na_2O \cdot 2CaO \cdot 3SiO_2$, while the compositions of the glasses studied in Refs. [12,13] are between the compounds $Na_2O \cdot 2CaO \cdot 3SiO_2$ ($N_1C_2S_3$) and $Na_2O \cdot CaO \cdot 2SiO_2$ ($N_1C_1S_2$), Fig. 1.

To evaluate the number of crystals per unit volume, $N(t)$, nucleated at a given temperature *versus* heat treatment time we employed the well-known Tammann or so-called 'development' method (see e.g. [5]). Then, $N(t)$ data were fitted into Collins's/Kashchiev's equation (2) [15,16]

$$\frac{N(t)}{I_{st}\tau} = \left[\frac{t}{\tau} - \frac{\pi^2}{6} - 2\sum_{m=1}^{\infty}\frac{(-1)^m}{m^2}\exp\left(-m^2\frac{t}{\tau}\right)\right] \quad (2)$$

to estimate the time-lag for nucleation, τ, and the steady-state value of the nucleation rate, I_{st}, as fitting parameters.

For sufficiently long times, this expression can be approximated by

$$N_V(t) = I_{st}(t - t_{ind}), \quad (3)$$

where

$$t_{ind} = \frac{\pi^2}{6}\tau. \quad (4)$$

Moreover, to obtain quantitative information about nucleation kinetics in the advanced stages of phase transformation the overall crystallization kinetics were analyzed with the JMAK equation:

$$\alpha(t) = 1 - \exp\{-Kt^n\}, \quad (5)$$

where α is the volume fraction transformed, n is the so-called Avrami coefficient, which can be estimated from the slope of a $\ln(-\ln(1-\alpha(t)))$ *versus* $\ln(t)$ plot. In the case of three-dimensional growth, the Avrami coefficient can be written as

$$n = \kappa + 3m, \quad (6)$$

where κ and m characterize the evolution of the crystal number ($N \sim t^{\kappa}$) and size ($D \sim t^m$) with time.

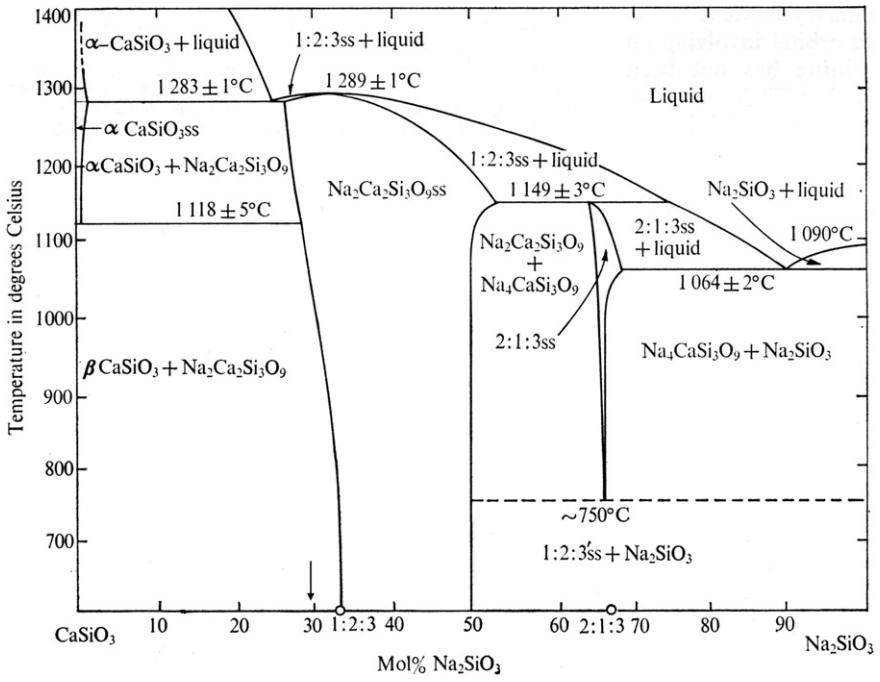

Fig. 1. Phase diagram of the pseudo-binary section $CaO \cdot SiO_2$–$Na_2O \cdot SiO_2$ of the sodium–calcium silicate system [14]. The arrow indicates the composition of the glass under investigation.

Well below the glass transition temperature, the crystals of stoichiometric composition $N_1C_2S_3$ and the solid solution crystals (between $N_1C_2S_3$ and $N_1C_1S_2$, with chemical formula $Na_{4+2x}Ca_{4-x}[Si_6O_{18}]$, $0 < x \leqslant 0.5$) show a reversible polymorphic transition at a temperature T_{pm}, which is accompanied by easily distinguished thermal effect on a DSC curve [17]. Since T_{pm} depends on the value of x, its variation was used to detect changes of the crystal composition during phase transformation.

An EDS (Stereosxcan 440) – dot map technique – was employed for the qualitative estimate of the compositional difference between the glassy matrix and crystals using $U = 20$ kV and $I = 1.5$ na. The measurement time for each point in the dot map was about 0.2 ms.

To visualize the diffusion zones around the growing crystals special multi-stage crystallization heat treatments were performed.

3. Results

3.1. Nucleation kinetics

Fig. 2 shows the typical $N(t)$ dependence used to estimate the time-lag (or the induction period t_{ind}) for nucleation and the steady-state nucleation rate I_{st}. Solid and dashed lines are plotted with Eqs. (2) and (3), respectively, using the parameters τ and I_{st} obtained by mathematical fitting (see Section 2). It should be noted that the 'development' method allows one to estimate the nucleation rate in the very early stages of the phase transformation when the volume of crystalline phase is negligibly small. Fig. 3 presents the steady-state nucleation rate (a) and the induction period (b) as functions of temperature.

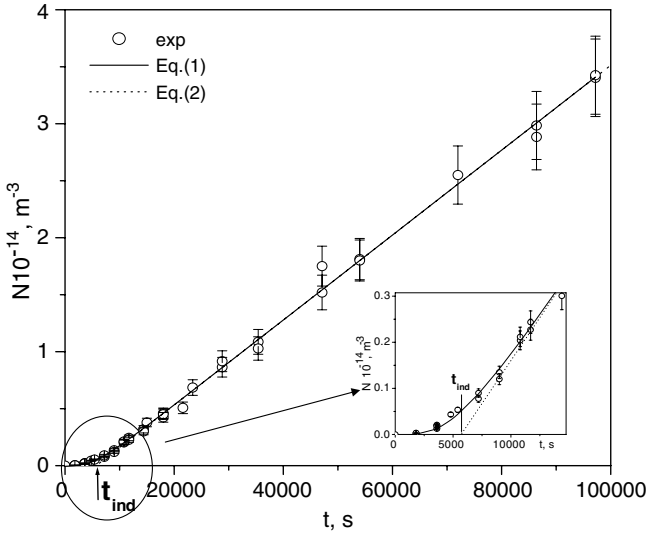

Fig. 2. Crystal number density *versus* time of nucleation at $T = 610$ °C estimated via the 'development' method. The inset shows the $N \sim t$ data on a larger scale. The solid and dashed lines were plotted with Eqs. (2) and (3), respectively.

3.2. Overall crystallization kinetics and crystal growth

Fig. 4(a) shows the crystallized volume fractions estimated by optical microscopy as a function of heat treatment time at $T = 610$ °C, which is close to the temperature T_{max} of the maximum nucleation rate $I_{max} \equiv I_{st}(T_{max})$ (see Fig. 3). The first experimental points correspond to times that

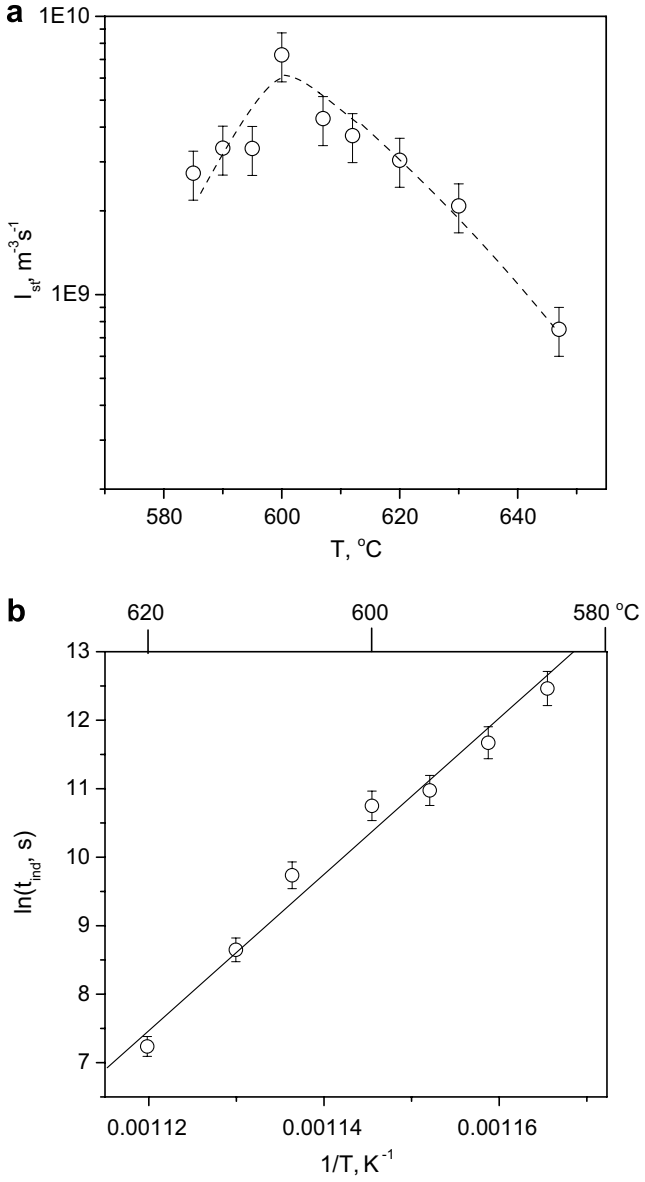

Fig. 3. Temperature dependencies of the steady-state nucleation rate (a) and induction period for nucleation (b).

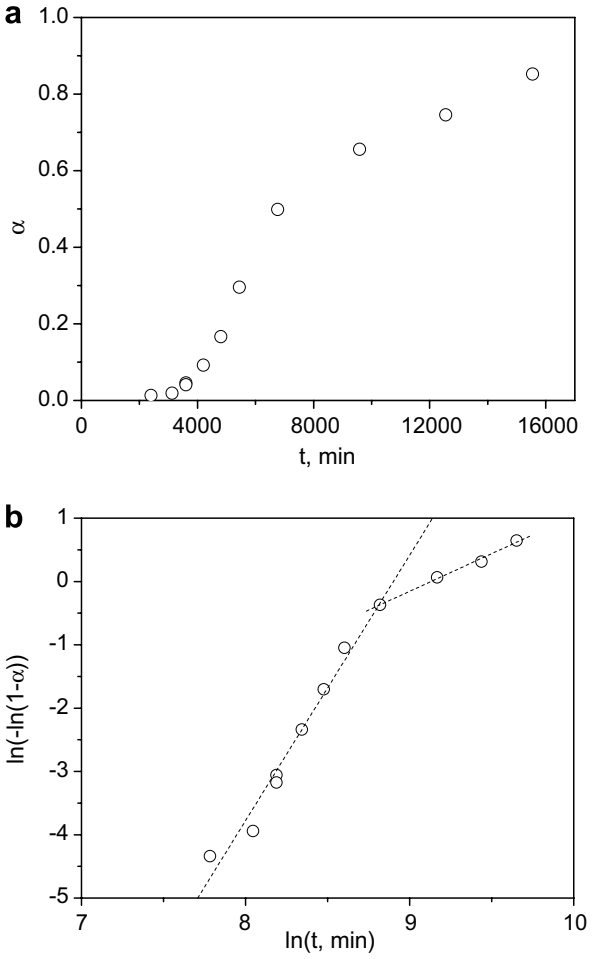

Fig. 4. Kinetics of overall crystallization at $T = 610\,°C$ (a) and the respective Avrami plot (b). The lines were obtained by least-squares linear fits.

strongly exceed the period investigated by the 'development' method (see Fig. 2). An Avrami plot is shown in Fig. 4(b).

The crystal growth kinetics at the same temperature (610 °C) is shown in Fig. 5 in normal (a) and logarithmic (b) coordinates. Fig. 6 shows the increase of crystal size at $T = 710\,°C$ for different crystal number densities. Since the nucleation rates are very small at $T = 710\,°C$, preliminary nucleation heat treatments were performed to change the crystal number density. In all cases the crystal size distributions were close to monodisperse. Lines represent approximations via the equation $D = At^m$.

3.3. Thermal analysis and reversible polymorphous transition

DSC heating and cooling curves are shown in Fig. 7. After crystallization from the liquid state the crystalline phase undergoes a reversible (exothermic) polymorphic transition at a temperature T_{pm} (well below the glass transition temperature). Fig. 8 presents T_{pm} taken from DSC heating-curves of partly crystallized samples *versus* volume fraction of crystalline phase.

3.4. The 'courtyard' phenomenon

Fig. 9 shows micrographs of glass samples subjected to a long single-stage treatment (a) at T_n (close to T_{max}), and to a triple treatment (b): first for a short time (30 min) at T_n to nucleate an appropriate number of crystals, then at $T_{gr} \gg T_{max}$ to grow them, and finally again at T_n for the same time as for the samples shown in Fig. 9(a). Thus this third treatment differs from the single-stage treatment only by the presence of previously formed large crystals.

3.5. EDS results

Fig. 10 shows a scanning electron microscopy (SEM) micrograph of crystals in a glass sample subjected to the

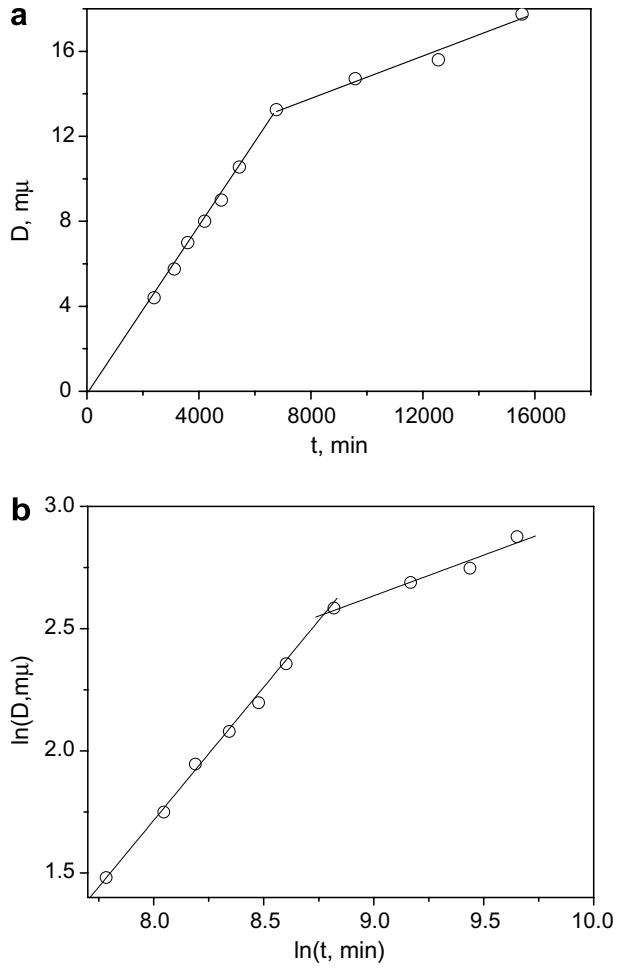

Fig. 5. Diameter of the largest crystals as a function of heat treatment time at $T = 610$ °C in linear (a) and logarithmic (b) coordinates. The lines were obtained by least-squares linear fits.

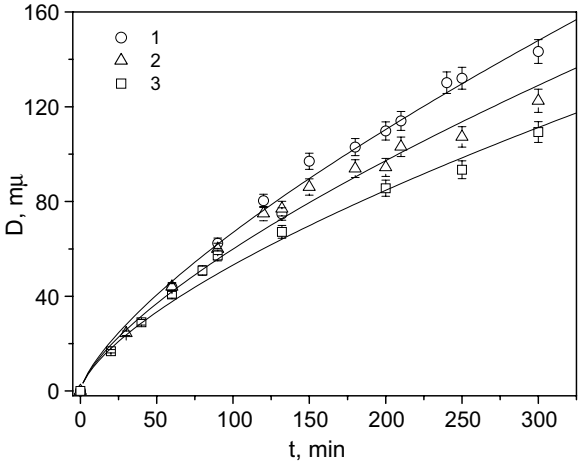

Fig. 6. Crystal diameters *versus* heat treatment time at $T = 710$ °C for different crystal number densities $N = 250$ (1), 1200 (2) and 4400 mm^{-3} (3). The lines were fit to $D = At^m$.

same triple treatment as the sample shown in Fig. 9(b). The line at the bottom shows the change of sodium content in arbitrary units (estimated via EDS) along the section

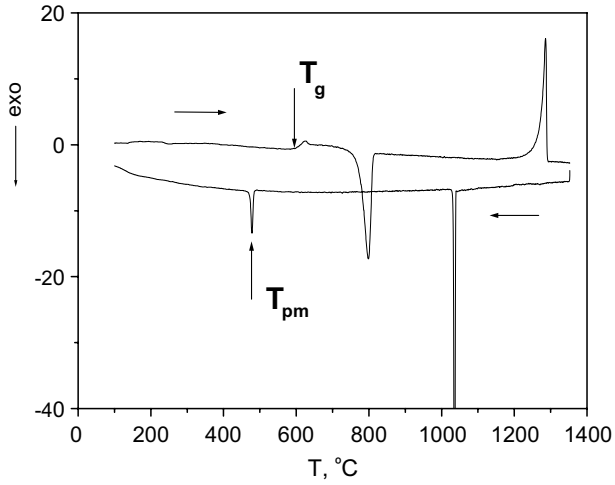

Fig. 7. Heating and cooling DSC curves: with cooling and heating rates $|q| = 10$ grad/min. The weight of the monolithic sample was about 40 mg.

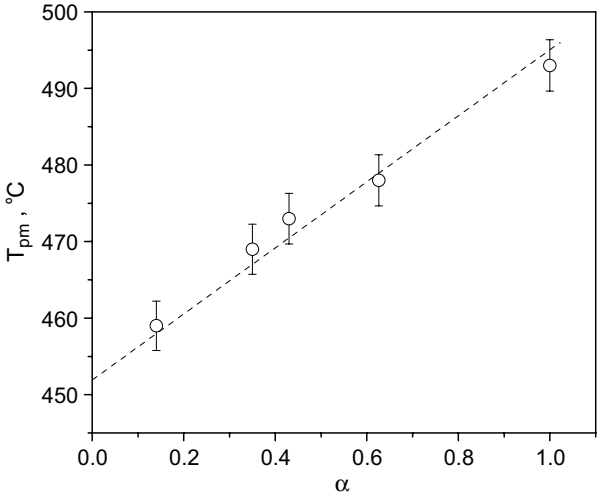

Fig. 8. Temperature of reversible polymorphic transition taken from heating DSC curves *versus* volume fraction crystallized at $T = 706$ °C. The dashed line is a linear fit.

shown in the top line. The relative content of sodium in the glassy matrix and crystalline phase is shown by a dot map in Fig. 11(b). This figure refers to a partly crystallized glass sample (Fig. 11(a)) having a thermal history similar to that of the sample shown in Fig. 9(b), with exception of the second heat treatment.

4. Discussion

The present results can be separated into two groups. The first one refers to nucleation at the early stages. In this case, when the crystallized volume fraction is very small, the possible difference between the crystal and liquid compositions does not have a remarkable influence on the glassy matrix composition. This situation is realized at low temperatures, typically at or below T_g (where crystal growth rates are very slow); or for short time intervals of

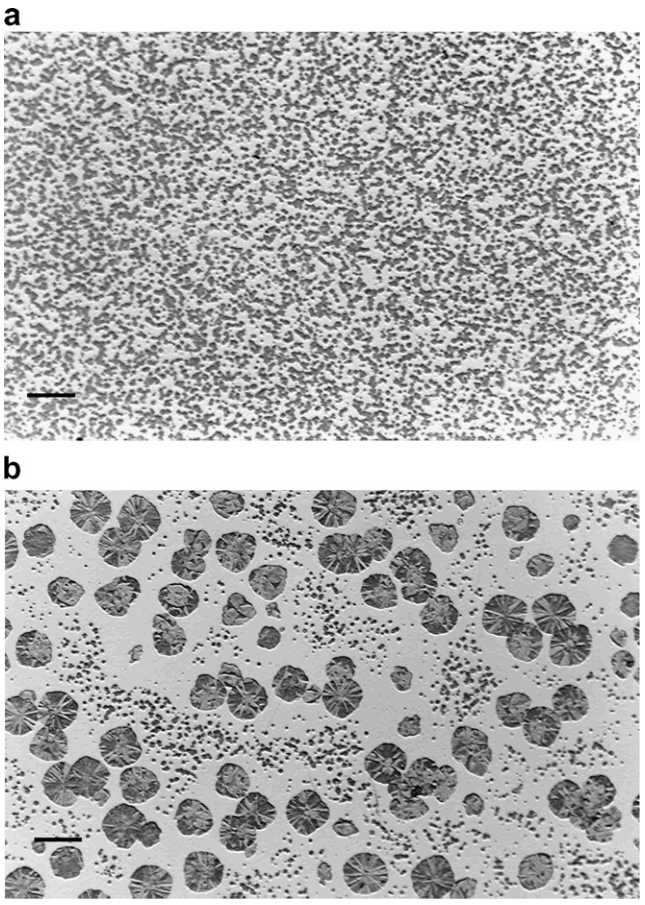

Fig. 9. Micrographs of glass samples subjected to a single heat treatment (a) at $T_n = 610$ °C for $t = 114$ h, and to a triple heat treatment (b) with the following sequence: $T_n = 610$ °C for $t = 30$ min + $T_{gro} = 706$ °C for $t = 214$ min + $T_n = 610$ °C for $t = 114$ h. The bars denote 100 μm.

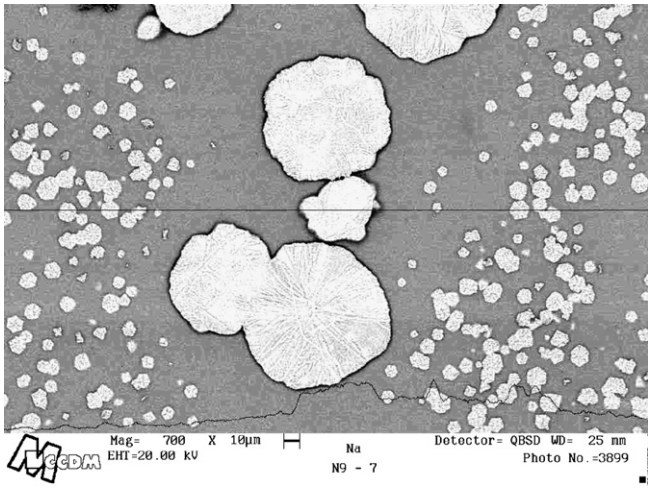

Fig. 10. SEM micrographs of a glass sample subjected to the following heat treatments: $T_n = 610$ °C, $t = 30$ min + $T_{gro} = 706$ °C, $t = 214$ min + $T_n = 610$ °C, $t = 114$ h. The bottom line represents the change sodium (in arbitrary units) along the straight line passing through the center.

crystallization treatment. The second group includes the results for the advanced stages of phase transformation

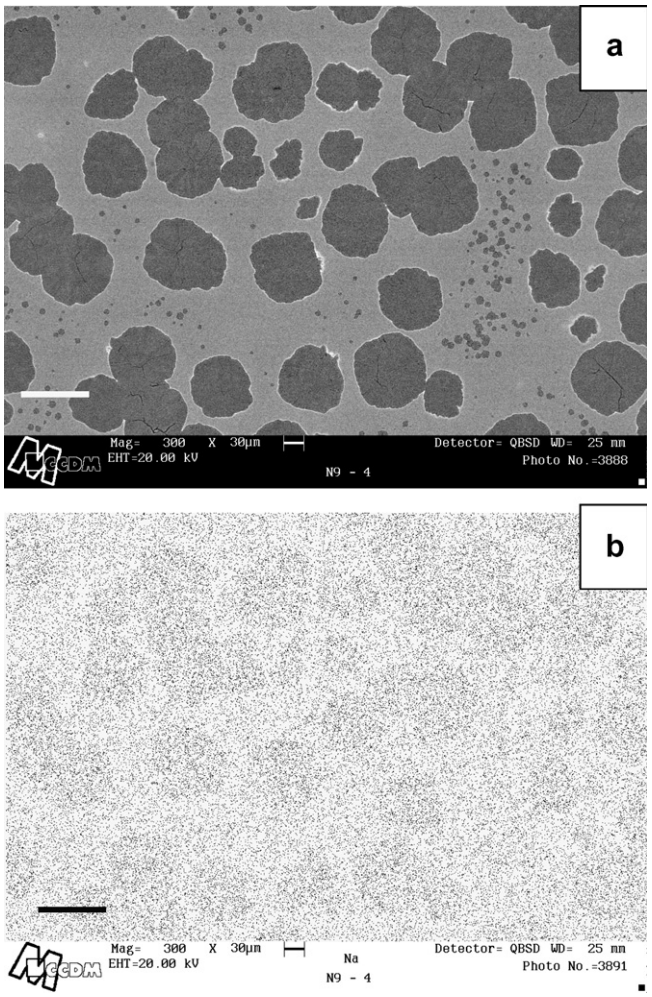

Fig. 11. SEM micrograph (a) and dot map (Na) (b) the same area of the glass sample subjected to the following heat treatments: $T_n = 610$ °C, $t = 30$ min + $T_{gro} = 706$ °C, $t = 274$ min + $T_n = 610$ °C, $t = 114$ h. The bars denote 100 μm.

(heat treatment at high temperatures or long treatments at low temperatures). These data could also shed light on the very beginning of crystallization (when the use of direct methods is difficult) since the early stages determine to a great extent the whole course of phase transition.

(i) Fig. 3(a) shows the typical temperature dependence of the steady-state nucleation rates, I_{st}, revealing the maximum, which results from an interplay between the thermodynamic and kinetic barriers. To discuss the maximum value of the nucleation rate $I_{max} = I_{st}(T_{max})$ we collected nucleation rates in sodium–calcium silicate glasses of compositions close to the metasilicate section of the phase diagram and plotted them *versus* the sodium oxide content C_{Na_2O}, Fig. 12(a), and the reduced glass transition temperature ($T_{gr} \equiv T_g/T_L$, T_L is the *liquidus* temperature), Fig. 12(b). The relatively monotonous decrease in I_{max} with decreasing C_{Na_2O} accelerates at a composition close to $N_1C_2S_3$. This peculiarity is absent in

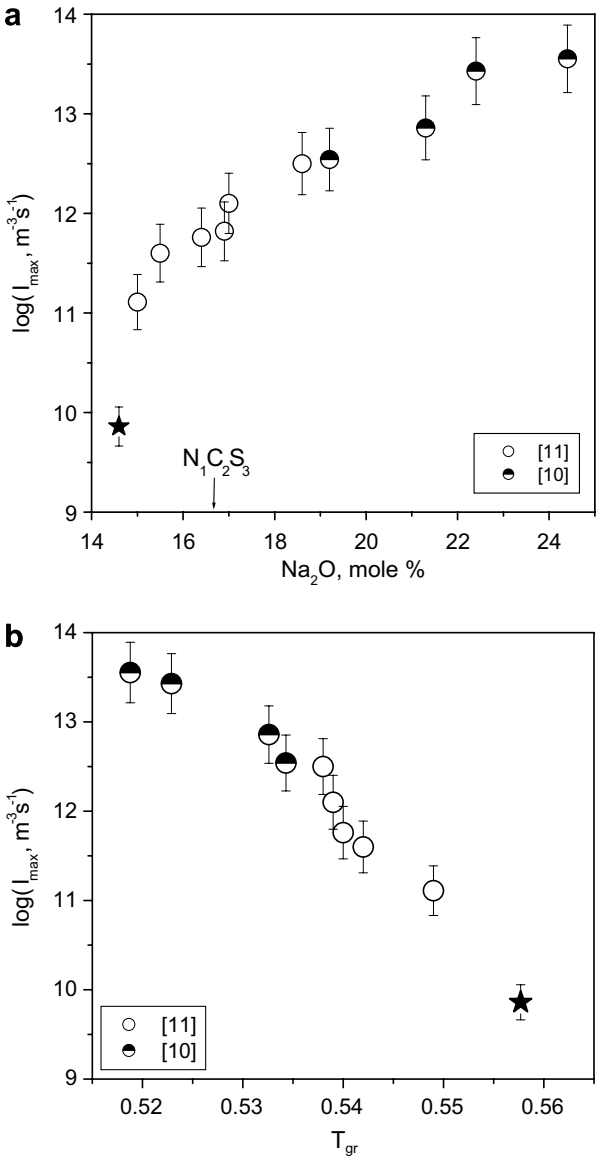

Fig. 12. Maximum steady-state nucleation rate in sodium–calcium metasilicate glasses *versus* sodium oxide content (a) and reduced glass transition temperature (b).

the $I_{max}(T_{gr})$ dependence, which clearly demonstrates a strong correlation between I_{max} and T_{gr}, that has been discussed in detail in Ref. [18]. This correlation indicates that with the increase of T_{gr} the kinetic inhibition of nucleation proceeds at higher temperatures corresponding to a higher thermodynamic barrier for nucleation (owing to the lower values of the thermodynamic driving force). Such correlation is much more pronounced when the nucleation rates refers to the same or similar crystal phases, since the thermodynamic barrier also depends on the melting enthalpy, the difference between the heat capacities of melt and crystal, and surface energy. This is the case shown in Fig. 12(b) where all nucleation rates refer to solid solutions based on the $N_1C_2S_3$ structure. It should be stressed that the nucleation rates shown in Fig. 12 (obtained by the 'development' method) refer to a stage when the crystals have about critical size and hence α is still negligible.

(ii) A significant prolongation of the heat treatment time, even at the lowest temperatures, allows one to study the overall crystallization kinetics. The kinetics of overall crystallization at $T = 610\,^{\circ}C$ is shown in Fig. 4. The $N(t)$ plot at this temperature for relatively short times is presented in Fig. 2. The respective Avrami plot (Fig. 4(b)) can be separated into two parts – before and after 6765 min, see the Avrami coefficients listed in Table 1. Crystal growth in the indicated time intervals (Fig. 5(b)) can be described as $D \sim t^m$, where m is shown in Table 1. This table also includes the values of κ estimated via Eq. (6). As follows from Table 1, for times below 6765 min the overall crystallization kinetics ($n \sim 4$) correspond to nucleation and growth with constant rates. For $t > 6765$ min the overall crystallization kinetics is controlled *only* by crystal growth, since the values of n and m reduce up to about 1 and 0.3, respectively. This means that at ~6765 min the nucleation process is practically terminated ($\kappa \ll 1$).

It is natural to assume that suppression of nucleation is caused by the exhaustion of sodium in the glassy matrix due to the compositional difference between the parent glass and growing crystals, as it was the case for glasses with compositions between $N_1C_2S_3$ and $N_1C_1S_2$ [7] in which sodium-rich solid solution crystals nucleated. In contrast to the latter case, however, in the glass here investigated (see Fig. 1) the formation of the stable phase $N_1C_2S_3$ as well as of sodium-rich solid solution crystals has to lead to sodium depletion causing a change in the crystallization kinetics. The change of the polymorphic transition temperature T_{pm} (Fig. 8) evidences the variation of the crystal composition during the course of crystallization. This change allows us to conclude that the starting crystal (critical nucleus) composition is *not* equal to $N_1C_2S_3$. Indeed according to the T_{pm} (Na_2O) dependence shown in Fig. 13, the initial crystal composition has about 18 mol% Na_2O (36 mol% Na_2OSiO_2) just right hand side of the $N_1C_2S_3$ compound in the phase diagram, and is thus *remarkably different from that of the parent glass*, which has 14.6 mol% Na_2O.

Similar results were obtained for a glass with 13.8 mol% Na_2O, for which we plotted the dependence of T_{pm} on the volume fraction crystallized (see Fig. 14). An estimate of

Table 1
Avrami exponent, n, crystal growth exponent m, $D \sim t^m$, crystal number exponent κ, $N \sim t^{\kappa}$

t (min)	n[a]	m	κ
<6765	4.2 ± 0.3	1.1 ± 0.1	~1
>6765	1.2 ± 0.1	0.3 ± 0.1	≪1

[a] $n = 3m + \kappa$.

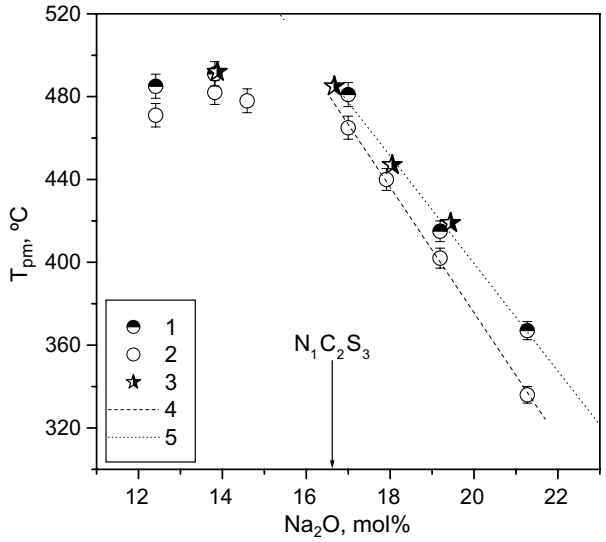

Fig. 13. Temperature of reversible polymorphic transition taken from DSC (1, 2) *versus* sodium oxide content at C_{SiO_2} close to 50 mol%. 1, 3 – heating and 2 – cooling with rate 10°/min. Dashed and doted lines are linear fits of experimental data (for glasses containing more than 16.6 mol% sodium oxide). 3 – data taken from Ref. [19].

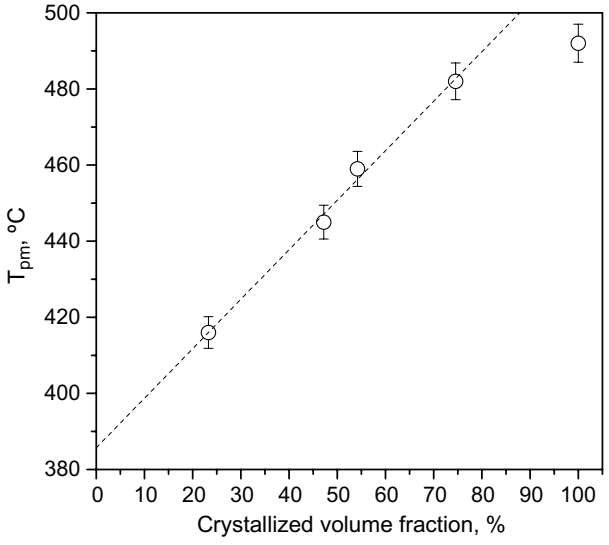

Fig. 14. T_{pm} of crystals *versus* volume fraction crystallized at $T = 650$ °C of a glass with composition $13.8Na_2O$–$35.4CaO$–$50.8SiO_2$ (mol%) by analysis. The dashed line is a linear fit of the experimental points with exception of the data corresponding to $\alpha = 100\%$.

the critical nuclei composition via variation of T_{pm} was also performed for a glass with 17 mol% Na_2O. Fig. 15 shows the sodium content in the critical nuclei estimated by extrapolation of the $T_{pm}(\alpha)$ plots to $\alpha = 0$, and by EDS measurements, previously performed by us [20], *versus* sodium content in the parent glasses. The data obtained via T_{pm} agree within the error limits with EDS measurements. One should recall that the parent glass and a fully crystallized sample were used in Ref. [20] as standards. According to Fig. 15 crystallization begins with nucleation

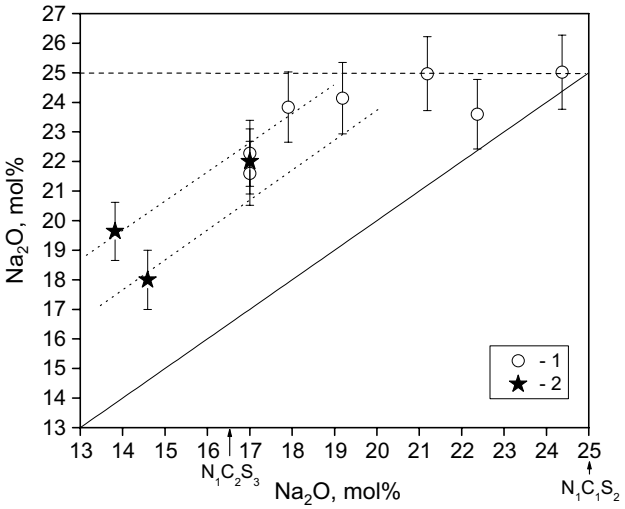

Fig. 15. Sodium oxide content in the critical nuclei *versus* sodium oxide in the parent glasses. Estimate by EDS (1) [20] and T_{pm} measurements (2). The solid line corresponds to the case when the compositions of the critical nuclei are equal to those of the respective parent glasses.

of solid solution crystals enriched in sodium as compared to the stoichiometric composition $N_1C_2S_3$ and the parent glass compositions. It is true for glasses with composition just left of $N_1C_2S_3$ and from the $N_1C_2S_3$–$N_1C_1S_2$ interval that leads to solid solution formation. As we have shown early, in the case of glasses of the $N_1C_2S_3$–$N_1C_1S_2$ interval, during crystallization the composition of the solid solution crystals reach that of the parent glass, i.e. at relatively low crystallization temperature the system arrives to its equilibrium corresponding to its phase diagram.

Another situation is verified for glasses just left of $N_1C_2S_3$. An X-ray analysis of fully crystallized materials with 14.6 mol% Na_2O treated at 607 °C did not reveal any $CaO \cdot SiO_2$. But according to the equilibrium phase diagram (Fig. 1) about 4 vol.% of this phase should form at some late stage. To confirm this result we crystallized at 650 °C the glasses with 13.8 and 12.4 mol% Na_2O (up to 100 and 98.6 vol.% crystalline phase), increasing in such a way the expected volume fraction of $CaO \cdot SiO_2$ up to 6% and 10%, respectively. However the new X-ray analysis did not reveal again any $CaO \cdot SiO_2$ crystal phase. This result means that the crystalline phase is sodium depleted solid solution. The continued slow increase of the T_{pm} of crystals containing less than 16.6 mol% sodium oxide (Fig. 13) also gives indirect evidence for formation of a solid solution since, if the stoichiometric phase $N_1C_2S_3$ precipitated the value of T_{pm} would not vary. According to the phase diagram (Fig. 1), a sodium depleted solid solution is stable at temperatures higher than about 1050 °C and thus should decay at temperatures as low as 607 and 650 °C into $N_1C_2S_3$ and $CaO \cdot SiO_2$. However this decomposition could be suppressed by kinetic reasons. Thus glasses with compositions just left of $N_1C_2S_3$, fully crystallized at low temperatures are composed by solid solutions, which are metastable with respect to $N_1C_2S_3$. It should be noted that

in the case of $BaO \cdot 2SiO_2$ glass crystallization at low temperatures the high-temperature form of barium disilicate, which is metastable at the temperatures corresponding to the maximum nucleation rates [21] first precipitates. One should also recall the formation of enstatite in $Mg_3Al_2Si_3O_{12}$ glass [22] instead of the equilibrium assemblage forsterite + sapphirite + cordierite.

The difference in sodium content between the parent glass and nucleated crystals must result in the formation of sodium depleted diffusion zones around crystals in the glassy matrix. These zones can be visualized via multi-stage heat treatment, as shown in Fig. 9(b). The region adjacent to the large crystals (preliminary grown at a relatively high temperature T_{gro}) is exhausted in sodium. This is the reason why during subsequent heat treatment at T_n (close to T_{max} of the parent glass) nucleation is strongly suppressed as compared with a glass subjected to only a single heat treatment (see Fig. 9(a)). Please recall that based on the dependence presented in Fig. 12 one can expect a strong decrease in the nucleation rate with decreasing $C_{Na_2O} < 14.6$ mol%.

The difference in sodium between the glassy matrix and the crystals was corroborated by qualitative EDS measurements. Fig. 10 presents a SEM micrograph of the glass sample subjected the same heat treatment as the one shown in Fig. 9(b). The bottom line represents the variation of sodium along the straight line shown above, which crosses the glassy matrix and the crystals. The X-ray dot map of Na of a similar sample also demonstrates enrichment of the crystals in sodium as compared with the glassy matrix, Fig. 11.

Since the crystal growth rate depends on the glass composition, it must also be affected by the change in the glassy matrix composition, which, as was shown earlier, practically stops nucleation in the advanced stages of phase transformation. During crystallization the sodium depleted glassy matrix undergoes an increase of viscosity. Hence deceleration of the growth kinetics could be expected with increase of the crystal number density due to the enhanced competition for sodium between the growing crystals, and the viscosity increase. According to Fig. 6 such slowdown indeed takes place. Moreover, Fig. 16 clearly shows an increase in the time exponent ($D = At^m$) with increasing average distance L between crystals estimated via the crystal number density, N, as $(1/N)^{1/3}$. However, an analysis of the m value and growth mechanism is not trivial and needs further investigation, since during growth both crystal and glassy matrix compositions change.

Summarizing the above results, we conclude that crystallization of a glass with composition corresponding to the two-phase region ($CaO \cdot SiO_2 + Na_2O \cdot 2CaO \cdot 3SiO_2$) of the $CaO–SiO_2–Na_2O$ equilibrium phase diagram *starts* with nucleation of a *sodium-rich solid solution* (as compared with the stoichiometric composition $N_1C_2S_3$ and to the parent glass composition). This compositional deviation must decrease the thermodynamic driving force. Hence, we suppose that the specific surface energy of the solid solution critical nuclei is smaller than that of the stable

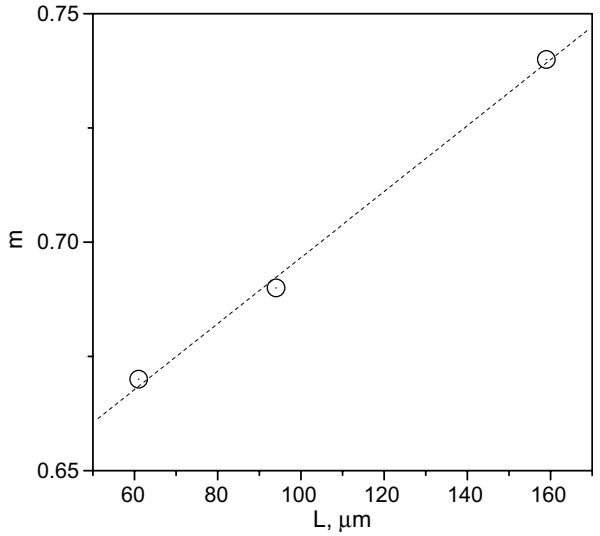

Fig. 16. Parameter m *versus* average distance between the growing crystals.

phase $N_1C_2S_3$ in such a way that it compensates for the reduction of the thermodynamic driving force, leading to a decrease in the thermodynamic barrier for nucleation.

The compositional deviation of critical nuclei from that of the evolving stable macro-phase not only agrees with the mentioned above experimental findings but also is corroborated by recent theory of phase nucleation–growth kinetics (see e.g. [23–25]). Any nucleation theory is widely based on the very reasonable assumption that processes of nucleation and growth are realized as a rule via an evolution path passing the saddle point of the respective thermodynamic potential surface corresponding to the critical cluster size since deviations of such saddle point paths result in the considerable increase of activation energies for nucleation. The generalized Gibbs' approach [26] shows, in contrast to the classical Gibbs' method and in agreement with density functional computations and computer simulations, that the state of the critical clusters, corresponding to the saddle point of this thermodynamic potential surface, differs and as a rule significantly from the state of the newly evolving phase. The changes of the structure and composition of the critical clusters leads to a significant decrease of the work of critical cluster formation and hence to a significant increase of the theoretical estimates for the steady-state nucleation rates [25], explaining, in such a way, why classical nucleation theory, which is based on Gibbs' classical thermodynamic approach, underestimates as a rule the steady-state nucleation rate.

The deviation of the state of the critical clusters is essentially determined by thermodynamics and not by *kinetics*. However, the trajectory of evolution, i.e. how the critical cluster is reached, is different in dependence on the values of the partial diffusion coefficients of the different components. These differences are discussed in [27] and in more detail in [28].

Thus the explication given in [9] of the compositional deviation of critical nuclei observed in sodium calcium metasilicate glasses [7], which keeps also at initial stage of crystal growth, as result of kinetics due to high diffusivity of sodium as compared with that of calcium conflicts the theoretical results. Also, as was shown in [29] for $N_1C_2S_3$ glass, the effective diffusion coefficient estimated from crystal growth rates is closer to that of Ca than to Na. Moreover in the crystallized glasses with composition just right of $N_1C_1S_2$ from $N_1C_1S_2$–$N_2C_1S_3$ interval only $N_1C_1S_2$ crystals were detected [30] whereas according to [9] one could expect the formation of $N_2C_1S_3$ crystals as the first phase.

5. Conclusions

We demonstrated a well-defined correlation between the maximum nucleation rate of solid solutions $Na_{4+2x}Ca_{4-x}[Si_6O_{18}]$ and the reduced glass transition temperature for glasses with compositions close to the meta silicate $CaO \cdot SiO_2$–$Na_2O \cdot SiO_2$ pseudo-binary section corroborating the tendency observed in previous studies with other compositions.

We have shown that crystallization of a glass with composition close to the $CaO \cdot SiO_2$–$Na_2O \cdot SiO_2$ pseudo-binary section, being just left of $Na_2O \cdot 2CaO \cdot 3SiO_2$, does not start with nucleation of the stable crystalline phases $CaO \cdot SiO_2$ (CS) or $Na_2O \cdot 2CaO \cdot 3SiO_2$ (NC_2S_3), as one expects from the equilibrium phase diagram, but instead it starts with a $Na_{4+2x}Ca_{4-x}[Si_6O_{18}]$ ($0 < x < 1$) *solid solution* that is noticeably enriched in sodium as compared to $N_1C_2S_3$. During crystallization the average composition of this solid solution changes, and in the fully crystallized sample arrives at that of the parent glass. This solid solution is stable at temperatures higher than 1050 °C, but is metastable at the used temperatures. We thus confirm a continuous compositional change of the *crystals* during the course of crystallization, starting from the very early (nucleation) stage, an effect which has not been given proper attention in the past.

Acknowledgments

We express our appreciation of the funding provided by the Brazilian agency FAPESP, and our indebtedness to Dr A.A. Cabral for DSC measurements.

References

[1] W. Ostwald, Z. Phys. Chem. 22 (1897) 289.
[2] E.D. Zanotto, V.M. Fokin, Philos. Trans. R. Soc. London, A 361 (2002) 591.
[3] J. Deubener, R. Brückner, M. Sternitzke, J. Non-Cryst. Solids 163 (1993) 1.
[4] V.M. Fokin, N.S. Yuritsyn, E.D. Zanotto, J.W.P. Schmelzer, J. Non-Cryst. Solids 352 (2006) 2681.
[5] V.M. Fokin, E.D. Zanotto, J.W.P. Schmelzer, J. Non-Cryst. Solids 278 (2000) 24.
[6] V.M. Fokin, O.V. Potapov, C.R. Chinglia, E.D. Zanotto, J. Non-Cryst. Solids 258 (1999) 180.
[7] V.M. Fokin, O.V. Potapov, E.D. Zanotto, F.M. Spiandorello, V.L. Ugolkov, B.Z. Pevzner, J. Non-Cryst. Solids 331 (2003) 240.
[8] D. Tatchev, A. Hoell, R. Kranold, S. Armyanov, Physica B 369 (2005) 8.
[9] M. Roskosz, M.J. Toplis, P. Richet, J. Non-Cryst. Solids 352 (2005) 180.
[10] A.M. Kalinina, V.N. Filipovich, Glass Phys. Chem. 2 (1995) 97.
[11] G. Völksch, T. Kittel, F. Siegelin, H.-J. Kleebe, in: presented at XIX International Congress of Glass, Edinburgh, 2001.
[12] E.N. Soboleva, N.S. Yuritsyn, V.L. Ugolkov, Glass Phys. Chem. 30 (2004) 481.
[13] O.V. Potapov, V.M. Fokin, V.L. Ugolkov, L.Y. Suslova, V.N. Filipovich, Glass Phys. Chem. 26 (2000) 39.
[14] G.K. Moir, F.P. Glasser, Phys. Chem. Glasses 15 (1974) 6.
[15] F.C. Collins, Z. Electrochem. 59 (1969) 209.
[16] D. Kashchiev, Surf. Sci. 14 (1969) 209.
[17] H. Ohsato, Y. Takeuchi, I. Maki, Acta Cryst. B46 (1990) 125.
[18] V.M. Fokin, E.D. Zanotto, W.P. Schmelzer, J. Non-Cryst. Solids 321 (2003) 52.
[19] I. Maki, T. Sugimura, J. Ceram. Assoc. Jpn. 76 (1968) 144.
[20] V.M. Fokin, E.D. Zanotto, N.S. Yuritsyn, W.P. Schmelzer, J. Non-Cryst. Solids 352 (2006) 2681.
[21] A.H. Ramsden, P.F. James, J. Mater. Sci. 19 (1984) 2894.
[22] A.-M. Lejene, P. Richet, J. Geophys. Res. 100 (1995) 4215.
[23] J.W.P. Schmelzer, J. Schmelzer Jr., I.S. Gutzow, in: J.W.P. Schmelzer, Gerd Röpke, Vyutcheslav B. Priezzhev (Eds.), Nucleation Theory and Application, JINR, Dubna, 1999, p. 237.
[24] J.W.P. Schmelzer, V.G. Baidakov, G.Sh. Boltachev, J. Chem. Phys. 119 (2003) 6166.
[25] J.W.P. Schmelzer, V.G. Baidakov, G.Sh. Boltachev, J. Chem. Phys. 124 (2006) 194503.
[26] J.W.P. Schmelzer, in: J.W.P. Schmelzer (Ed.), Nucleation Theory and Application, Wiley-VCH, Berlin-Weinheim, 2005, p. 447.
[27] J.W.P. Schmelzer, A.S. Abyzov, J. Möller, J. Chem. Phys. 121 (2004) 6900.
[28] J.W.P. Schmelzer, in: Proceedings of the 11th International Conference on the Physics of Non-Crystalline Solids, Rhodes, Greece, 2006, J. Non-Cryst. Solids, submitted for publication.
[29] N.S. Yuritsyn, in: J.W.P. Schmelzer, G. Röpke, V.B. Priezzhev (Eds.), Nucleation Theory and Applications, Joint Institute for Nuclear Research, Dubna, 2006.
[30] N.S. Yuritsyn, personal communication, St. Petersburg, 2006.